ES Energy & Environment

REVIEW PAPER View Article Online

Electrolytic Carbons from CO_2 and Their Applications

Ping Peng,[1] Ao Yu,[1] Jiawen Ren[2*] and Fangfang Li[1*]

Tremendous efforts have been paid to tackle our energy crisis and environmental issues. CO_2 as main source for the greenhouse effect, is very abundant in nature and can be used as feedstock to prepare value-added carbon materials via electrochemical reduction. By carefully manipulating electrolysis current density, electrolyte composition, electrode materials and temperature, various functional carbon materials, including carbon nanotubes (CNTs), graphene, graphite, nanodiamonds, etc., could be readily generated with high Faraday Efficiency. As-obtained materials exhibits excellent performances in energy applications like batteries and supercapacitors. Electrochemical reduction of CO_2 provides a promising pathway for CO_2 capture and conversion and creates materials suitable for high energy power/density devices.

Keywords: CO_2 reduction; Carbon nano-structures; Molten salt; Electrolytic

Received 14 November 2018**, Accepted** 10 December 2018

DOI: 10.30919/esee8c205

1. Introduction

The rising levels of atmospheric carbon dioxide, predominantly because of anthropogenic activities such as fossil fuel burning,[1] is threating the sustainable development of the society. The globe climate change, mainly due to the increased CO_2 concentration,[2] has attracted plenty of attention to develop technologies that can achieve a reduction of atmospheric CO_2 to a sustainable level. Despite of the fact that plants can absorb CO_2 by photosynthesis process,[3] the decrease of CO_2 level is still impossible by plants compared to the high speed of population increase and expanded industry. Many efforts have been made on the capture of carbon dioxide and conversion into CO,[4-6] formic acid,[7] alcohols,[8-10] and hydrocarbons,[11-13] methane[14] by a chemical way, such as hydrogenation reaction. In these conversion processes, CO_2 acts as the chemical feedstock for the manufacturing of valuable chemicals, however, these routes for CO_2 conversion are bottle-necked by the cost, such as expensive catalysts, which hinders the development of these methods.

In contrast, liquid-phase electrochemical reduction of CO_2 into useful chemicals has been widely studied and reviewed recently by Paul. J Kenis[15] and Jiujun Zhang.[16] The standard reduction potential of CO_2 is very close to hydrogen evolution but it has a low solubility in aqueous solution. Thus, in many cases, hydrogen evolution is predominant. The low Faraday efficiency as well as further gas separation makes this process still far away from commercialization. Room temperature ionic liquids (RTILs) with wide electrochemical window and high solubility of CO_2 have been studied for CO_2 reduction, but the high cost and toxicity of RTILs hamper their further commercial applications.[11,17,18] In contrast to these electrolytes, molten salts render low cost, low toxicity and high ionic conductivity with a low vapor pressure, and have been proven as practical electrolytes for capture and electrochemical reduction/splitting of CO_2.[19] This method relies on the reduction of dissolved CO_2 between two biased electrodes, where either solid carbon, generally formed below 850 °C, or CO, when >950 °C, is deposited at the cathode, with very high coulombic efficiency.[20,21] In temperature between, carbon and CO are co-synthesized at cathode. The reaction at cathode is either Eq. (1) or Eq. (2). However, it should be noted that carbon could be generated by direct electrolysis of CO_2 either at room temperature or melting salts, but high pressure is required in both cases.[22] The reaction is as listed in Eq. (3)

$$Co_3^{2-} + 4e^- \rightarrow C + 3O^{2-} \quad (1)$$

$$CO_3^{2-} + 2e^- \rightarrow CO + 2O^{2-} \quad (2)$$

$$CO_2 \rightarrow C + O_2 \quad (3)$$

The deposited carbons at cathodes, initially, were not received much attention. The discovery of fullerenes,[23,24] CNTs,[25] and graphene,[26,27] ignited tremendous interests on nano-carbons because of their unique features in electronics, mechanics, chemical properties and supramolecular chemistry.[28,29] These also put questions to the researchers on the possibility of generating such nano-carbons by electrolysis of CO_2 or carbonates. The recent efforts clearly demonstrated that nanocarbons like nanotubes,[30-33] nanofibers,[34] graphene,[35] nanodiamond,[36-38] nanographite[39] and hollow spheres[40] could be generated by direct or indirect reduction of carbon dioxide. The advanced features of this methodology are (1) the carbon properties, such as size, shape, surface

[1]*State Key Laboratory of Materials Processing and Die & Mould Technology, School of Materials Science and Engineering, Huazhong University of Science and Technology, Wuhan 430074, China*
[2]*Department of Chemistry, The George Washington University, Washington, DC 20052, USA*
***E-mail:** ren.jiawen@gmail.com; ffli@hust.edu.cn*

areas and defects could be tailored by the composition of electrolyte,[41-44] electrolysis temperature,[45,46] current density and the electrode materials;[41,47] a big variety of carbons could be produced;[45] (2) the B, S and P hetero-atoms could be in-situ doped simply by adding corresponding metal salts rather than to use organic or expensive chemicals as in wet-synthesis or gas-deposition method;[31,48-50] (3) the resulting materials have shown excellent performances in supercapacitors and batteries;[51-56] (4) the large-scale production is possible as indicated from prof. Licht's work,[57] promising technique for the CO_2 capture and conversions.

2. Thermodynamics of CO_2 reductions

As mentioned above, the electrochemical reduction of CO_2 at room temperature is relatively complicated, the products could be CO,[58] formate[59] or formic acid,[60] methanol,[61] or hydrocarbons,[12] depending on the electrolyte and catalysts used. The thermodynamic electrochemical half-reactions of CO_2 reduction and their associated standard electrode potentials are listed in Table 1.[16] It is worthy to mention that the reactions listed in Table 1 are thermodynamic, for aqueous solutions, giving indication of each reaction's tendency and possibility but no indicating the reaction's kinetics, such as rate and mechanism. Although the carbon deposition needs higher voltage (E^0 = 0.21 V), meaning easier, than hydrogen evolution (E^0 = 0 V) reaction, the kinetics problems make the later one is predominant in most cases. The studies to solve the problems of sluggish reduction rate, low selectivity (multi-products) and high overvoltage are on-going by many groups, mainly focusing on the production of hydrocarbons or methanol or CO, though pure carbon could be generated with high pressure of CO_2 in non-aqueous electrolyte, as shown in the next section.

In molten carbonates, the reactions happened also had a debate for a long time. Recent progress stepped further on the verification of the reactions. In most experiments, one of Li_2CO_3, Na_2CO_3, K_2CO_3, $CaCO_3$, and $BaCO_3$, or a mixture of above was involved and the reactions during electrolysis are directly dependent on the electrolyte used. In pure Na_2CO_3 or K_2CO_3, or corresponding mixture, results from several group suggested the metal was deposited, and the cathode would get burning whenever contact with air.[62] Based on these results, the reaction in this system probably is either Eq. (4) or (5).

$$Na_2CO_3 \rightarrow 2Na + CO + O_2 \quad (4a)$$

$$2Na_2CO_3 \rightarrow 4Na + 2CO_2 + O_2 \quad (4b)$$

$$K_2CO_3 \rightarrow 2K + CO + O_2 \quad (5a)$$

$$2K_2CO_3 \rightarrow 4K + 2CO_2 + O_2 \quad (5b)$$

When $CaCO_3$ is the main component of an electrolyte, e.g., Ca/Ba, Ca/Na, Ca/K or Ca/Na/K carbonate, the main reaction supposed to be Eq. (6). The reason is that

$$3CaCO_3 \rightarrow 3CaO + C + 2CO_2 + O_2 \quad (6)$$

CaO has a very limited solubility in the molten carbonates and would precipitate immediately after generation, which lead to a shortage of oxygen ions (O^{2-}) at anode and therefore the reaction (7) is dominated at anode. This conclusion was further confirmed by our group's experiments.[31] Two experiments were conducted, one was

$$2CO_3^{2-} \rightarrow 2CO_2 + O_2 + 4e \quad (7)$$

with pre-mixed carbonate electrolyte, containing $CaCO_3$ and Li_2CO_3, the other one was adding solid $CaCO_3$ into Li_2CO_3 melt during electrolysis. CaO precipitated directly at cathode in the first experiment, while CaO precipitated at the bottom of the container in the second. This is because Ca^{2+} ions distributed evenly in a pre-mixed electrolyte, while Ca^{2+} ions mainly present around the $CaCO_3$ powder in the later experiment. The generated cathodic Li_2O, which is high soluble in molten carbonates, diffused to anode and was captured by Ca^{2+} ions and sedimented at the bottom of container. It should be noted that this conclusion is only

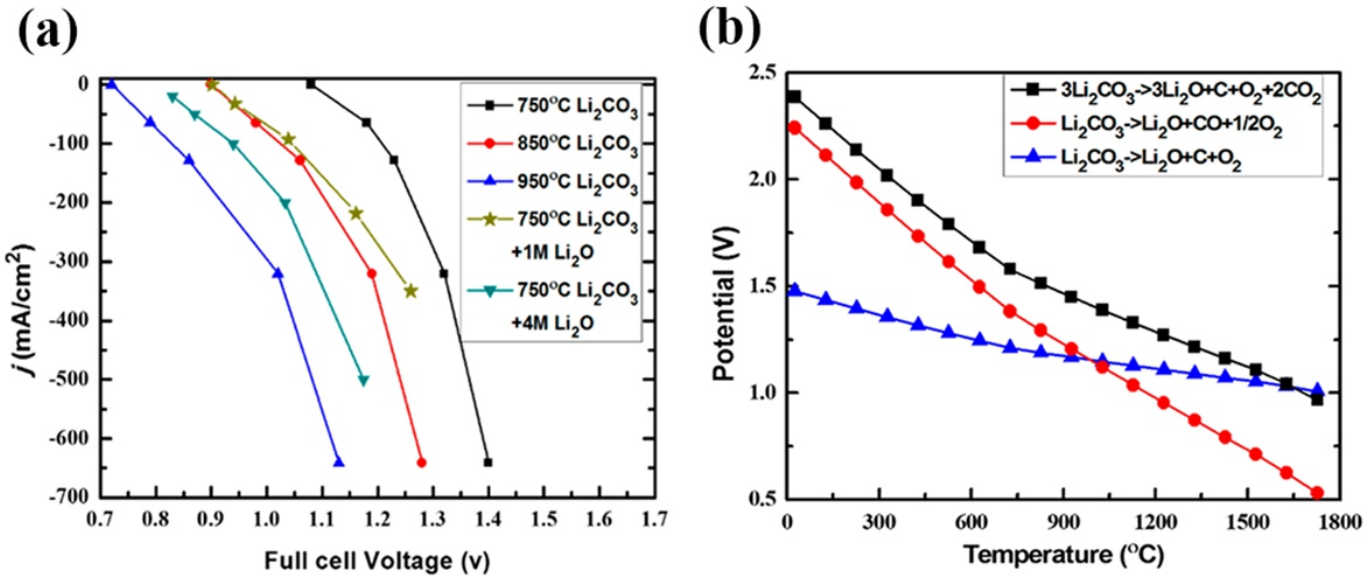

Fig. 1 Experimental results vs thermodynamic calculations. (a) Experimental full cell potentials with Ir and steel as the anode and cathode, respectively; (b) Calculated standard potentials of carbon deposition or CO release reaction in pure Li_2CO_3 electrolyte. Reprinted with permission from Ref. 64. Copyright 2015, American Chemical Society.

Table 1 Selected standard potentials of CO_2 in aqueous solutions (V vs SHE) at 1.0 atm and 25 °C, calculated on the basis of the standard Gibbs energies of the reactants. Reprinted permission from ref. 16. Copyright 2014, Royal Society of Chemistry.

Half-electrochemical Thermodynamic reactions	Electrode potentials (V *vs*. SHE) under standard conditions
$CO_2(g) + 4H^+ + 4e^- = C(s) + 2H_2O(l)$	0.210
$CO_2(g) + 2H_2O(l) + 4e^- = C(s) + 4OH^-$	–0.627
$CO_2(g) + 2H^+ + 2e^- = HCOOH(l)$	–0.250
$CO_2(g) + 2H_2O(l) + 2e^- = HCOO^-(aq) + OH^-$	–0.1078
$CO_2(g) + 2H^+ + 2e^- = CO(g) + H_2O(l)$	–0.106
$CO_2(g) + 2H_2O(l) + 2e^- = CO(g) + 2OH^-$	–0.934
$CO_2(g) + 4H^+ + 4e^- = CH_2O(l) + H_2O$	–0.070
$CO_2(g) + 3H_2O(l) + 4e^- = CH_2O(l) + 4OH^-$	–0.898
$CO_2(g) + 6H^+ + 6e^- = CH_3OH(l) + H_2O(l)$	0.016
$CO_2(g) + 5H_2O(l) + 6e^- = CH_3OH(l) + 6OH^-$	–0.812
$CO_2(g) + 8H^+ + 8e^- = CH_4(g) + 2H_2O(l)$	0.169
$CO_2(g) + 6H_2O(l) + 8e^- = CH_4(g) + 8OH^-$	–0.659
$2CO_2(g) + 2H^+ + 2e^- = H_2C_2O_4(aq)$	–0.500
$2CO_2(g) + 2e^- = C_2O_4^{2-}(aq)$	–0.590
$2CO_2(g) + 12H^+ + 12e^- = CH_2CH_2(g) + 4H_2O(l)$	0.064
$2CO_2(g) + 8H_2O(l) + 12e^- = CH_2CH_2(g) + 12OH^-$	–0.764
$2CO_2(g) + 12H^+ + 12e^- = CH_2CH_2OH(l) + 3H_2O(l)$	0.084
$2CO_2(g) + 9H_2O(l) + 12e^- = CH_2CH_2OH(l) + 12OH^-$	–0.744

applicable in molten carbonate, different mechanisms may be possible in other melts depending on the solubility of CaO.

On the other hand, $BaCO_3$, also an alkaline earth metal carbonate, exhibited different behavior.[63] In the electrolyte of Ba, Ba/Na, Ba/K or Ba/Na/K molten carbonates, the main reaction is (8) due to the good solubility of BaO. However, the electrolysis in pure Li_2CO_3 or melts with Li_2CO_3 is relatively complicated.

$$BaCO_3 \rightarrow BaO + C + O_2 \quad (8)$$

Li_2O has a high solubility of up to 9 M/kg in Li_2CO_3. Thus, it is reasonable that the main reaction should be similar to Eq. (8), that is:

$$Li_2CO_3 \rightarrow Li_2O + C + O_2 \quad (9)$$

Unfortunately, the thermodynamic calculation results based on Eq. (9) (Fig. 1b) is much larger than the experimental results as shown in Fig. 1a.[64]

The presence of either Li_2O or CO_2, or increase the CO_2 pressure can further reduce the reaction potential in pure Li_2CO_3 electrolyte. The reaction was supposed by our group as Eq. (10).

$$xLi_2O + (1+x)CO_2 \rightarrow xLi_2CO_3 + C + O_2 \quad (10)$$

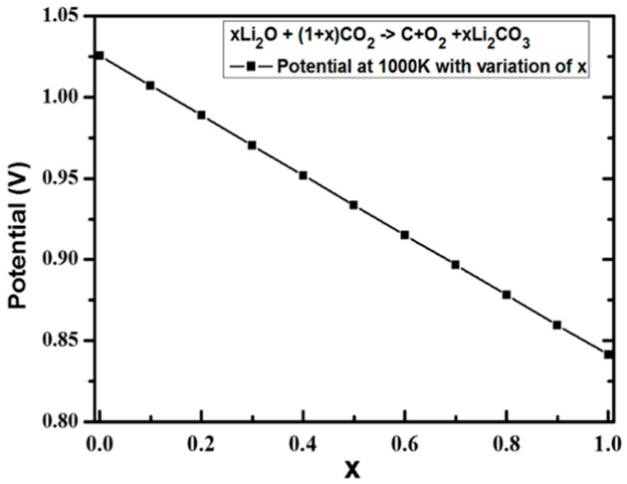

Fig. 2 Standard potentials of reaction (10) with variation of x. Reprinted with permission from Ref. 64. Copyright 2015, American Chemical Society.

Table 2 shows the calculated standard potentials of carbon deposition in different systems based on above reactions. The calculations are based on the Nernst Eq. $\Delta G^0 = - nE^0F$, where the ΔG^0, n, E^0, and F represent standard Gibbs free energy change, number of transferred electrons, standard reaction potential, and Faraday constant, respectively.

Another feature of the carbon deposition from carbonate is that hetero-atoms could be incorporated simply by adding corresponding salt into the melts. Table 3 shows some calculated standard potentials for the reference of possible doping element.

3. Directly CO_2 splitting

Although the potential of CO_2 splitting into carbon and oxygen is almost independent of temperature, ~1.02 V, from thermodynamic calculations, it was difficult to reduce CO_2 into carbon at room temperature in aqueous solution because of side reactions. Using ionic liquid 1-n-butyl-3-methylimidazoium hexafluorophosphate ([Bmim]PF_6) as the electrolyte and glassy carbon as the cathode, Lu *et al*.[65] carried out a series of studies on the electrochemical reduction of CO_2 at 25~100 °C under various CO_2 pressures (1~5 atm) The results show that the Faraday efficiency is directly related to the CO_2 pressure, higher pressure, better efficiency. The more interesting part is that the resulted product at cathode is a mixture of "carbon-nanotubes" of ~33 nm, nanographites, and amorphous carbons, as claimed by authors. However, it is still questionable that these "carbon-nanotubes" are tubular amorphous carbon or real carbon nanotubes due to the lack of further characterizations, e.g., Raman, TGA, etc. It may deserve to further study above results to confirm the product content, either in-situ products or after post-treatment of annealing.

Another study of direct CO_2 splitting was performed by Inessa Novoselova *et al*,[66] at high temperatures. The electrochemical behavior of metal halide molten salts (Na,K|Cl; Na,K,Cs|Cl), saturated with CO_2 under an excessive pressure of up to 1.5 MPa, has been investigated in the temperature range of 550–850 °C by cyclic voltammetry. An electrochemical-chemical-electrochemical (ECE) mechanism is proposed based on cyclic voltammetry (CV) results, and a mixture of carbon nano-particles of different forms and structures, *e.g.* crystalline graphite, blocks of amorphous carbon, carbon nanotubes (CNT) and nanofibers, were found at cathodic deposits. No estimation on the percentage of each is available in this report. The outer diameter of the tubes is 5–250 nm, and the internal diameter is 2–140 nm. One surprise is the existence of Fe (iron) in the deposits as shown in the XRD (Fig. 3c). This may be the reason of creation of CNTs as suggested by our reports[31,32,57] and chemical vapor deposition (CVD) methods,[67,68] The other interesting feature is that fullerene phase was detected when a halide melts of Na,K,Cs|Cl was used as the electrolyte. Further investigations may be needed to check out the possibility of synthesis of fullerene with high yield by CO_2 reduction, either direct or indirect electrolysis carbonates at low temperatures. Several reports are available on the electrochemical studies of halide melts with CaO under CO_2 flow.[22,30] But the mechanism is carbon dioxide reacted with CaO to form $CaCO_3$ which was further reduced as reaction (6). Therefore, this is not a direct CO_2 splitting and will be discussed in the next section.

4. Electro-reduction of carbonates into nanocarbons

As discussed above, the direct splitting of CO_2 could result in nanocarbons like CNTs, but lack of control. The products are mainly a collection of various carbon nanostructures. Moreover, it is difficult and dangerous in handling high pressure of CO_2. On the contrary, molten carbonates as storage materials of CO_2 are easily handled and the reaction set-up could be much simple. Several groups recently reported the selective synthesis of nanocarbons by electro-reduction of molten carbonates with high yield. For example, our group successful synthesized CNFs (carbon nanofibers)/CNTs from molten carbonate via a rational design inspired by chemical vapor deposition (CVD). The process is illustrated in Fig. 4.[31]

The CNTs were prepared by conducting the electrolysis between a 10 cm^2 coiled galvanized steel wire cathode (shown in Fig. 5)[34] and an oxygen generating nickel anode in 730 °C Li_2CO_3 melt. The electrolysis was initiated at a low current of 5 mA/cm^2 on cathode, then constant current electrolysis at high current (100 mA/cm^2) for 2 to 4 Ah. As shown in Fig. 5, the solid carbon was deposited on the cathode, which proved to be carbon nanofibers (CNFs). The bright points presented in SEM are metal nucleation points for carbon fibers growth and was

Table 2 Standard potentials of electro-reductions of molten carbonates calculated from thermodynamic data. The thermodynamic data are from Ishan Barin, Thermochemical data of pure substances, 1995, VCH.

T/K	E^o_{R3} /V	[b]E^o_{R11} /V	E^o_{R9} /V	E^o_{R4a}/V	E^o_{R4b} /V	E^o_{R5a}/V	E^o_{R5b}/V	E^o_{R6} /V	E^o_{R8} /V
298	-1.022	-1.333	-1.477	-2.360	-3.387	-2.403	-3.473	-2.040	-1.587
300	-1.022	-1.332	-1.476	-2.358	-3.385	-2.401	-3.470	-2.037	-1.586
400	-1.023	-1.287	-1.435	-2.262	-3.237	-2.301	-3.315	-1.915	-1.542
500	-1.023	-1.241	-1.395	-2.163	-3.086	-2.200	-3.159	-1.795	-1.499
600	-1.024	-1.195	-1.355	-2.066	-2.937	-2.100	-3.005	-1.676	-1.456
700	-1.024	-1.150	-1.316	-1.970	-2.791	-2.001	-2.853	-1.559	-1.413
800	-1.025	-1.104	-1.279	-1.876	-2.649	-1.904	-2.704	-1.443	-1.372
900	-1.025	-1.059	-1.242	-1.784	-2.509	-1.808	-2.557	-1.328	-1.330
1000	-1.026	-1.013	-1.208	-1.692	-2.371	-1.713	-2.413	-1.215	-1.289
1100	-1.026	-0.968	-1.185	-1.602	-2.236	-1.597	-2.225	-1.103	-1.250
1200	-1.026	-0.924	-1.163	-1.506	-2.088	-1.468	-2.012	-0.992	-1.215
1300	-1.026	-0.879	-1.142	-1.383	-1.887	-1.345	-1.812		-1.181
1400	-1.026	-0.834	-1.122	-1.261	-1.688	-1.225	-1.616		-1.148
1500	-1.027	-0.790	-1.102	-1.141	-1.492	-1.106	-1.423		

[a] Calculations based on graphite as the carbon product to calculate the above table.
[b]Standard potential of reaction (11) $CO_2 \rightarrow CO + 1/2O_2$
E^o_{RN} represents the standard potentials calculated by reaction N in the text. (N = 3,4a,4b, etc.)

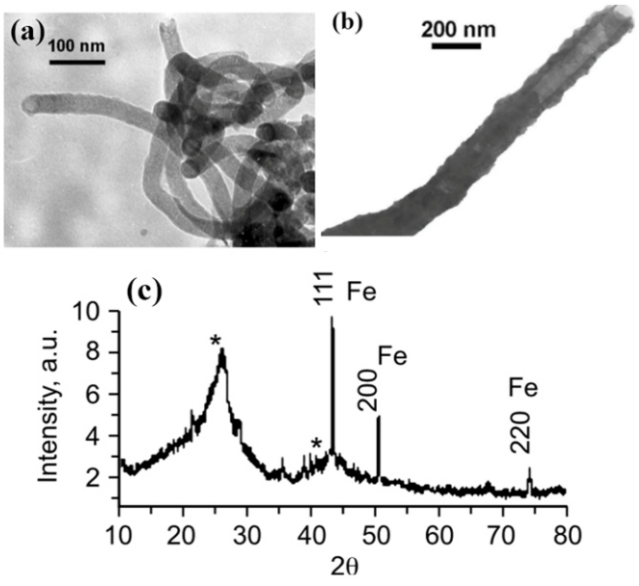

Fig. 3 (a,b) TEM images of black powders produced in the system of NaCl-KCl-CO_2, electrolysis conditions: P_{CO2} = 1.0 MPa; T = 750°C; i_k = 13.5, 42 mA/cm^2; (c) XRD of products at i_k = 42 mA/cm^2. Reprinted with permission from Ref. 66. Copyright 2008, Walter de Gruyter GmbH.

Table 3 Electro-reductions standard potentials of some lithium salts contain atoms other than carbon. (Only indicating each reaction's tendency and possibility but giving no indication of the reaction's kinetics, such as rate and mechanism.)

T/K	E^o ($2LiBO_2 \rightarrow Li_2O + 2B + 3/2O_2$)	E^o ($2LiAlO_2 \rightarrow Li_2O + 2Al + 3/2O_2$)	E^o ($Li_2SiO_3 \rightarrow Li_2O + Si + O_2$)	E^o ($Li_2SO_4 \rightarrow Li_2O + S + 3/2O_2$)
298	-2.356	-2.920	-2.582	-1.312
300	-2.355	-2.919	-2.581	-1.311
400	-2.312	-2.868	-2.534	-1.266
500	-2.268	-2.817	-2.487	-1.219
600	-2.224	-2.766	-2.441	-1.172
700	-2.181	-2.715	-2.394	-1.126
800	-2.138	-2.665	-2.348	-1.080
900	-2.095	-2.614	-2.302	-1.036
1000	-2.052	-2.561	-2.255	-0.988
1100	-2.010	-2.507	-2.210	-0.940
1200	-1.978	-2.452	-2.164	-0.894
1300	-1.949	-2.398	-2.118	-0.849
1400	-1.921	-2.344	-2.072	
1500	-1.893	-2.289	-2.028	

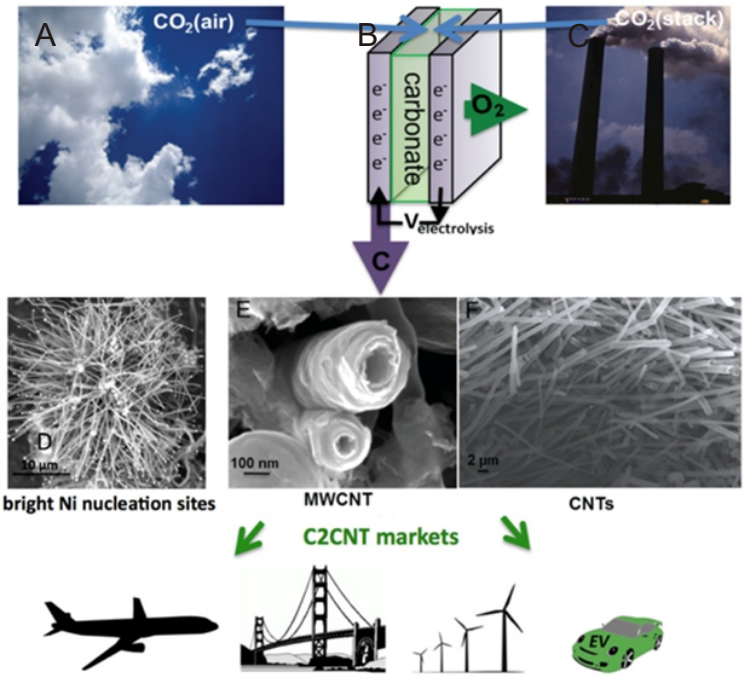

Fig. 4 Electrochemical synthesis of carbon nanostructures from CO_2 in molten lithium carbonate. (D) SEM image of the carbon nanostructures with nickel as nucleation sites. (E) High magnification SEM of the synthesized carbon nanotubes and (F) Low magnification SEM of as-synthesized CNTs. Bottom: Carbon materials were applied in lightweight jets, strengthened bridges, wind turbines, and electric vehicle body components and batteries. Reprinted with permission from Ref. 31. Copyright 2017, Elsevier.

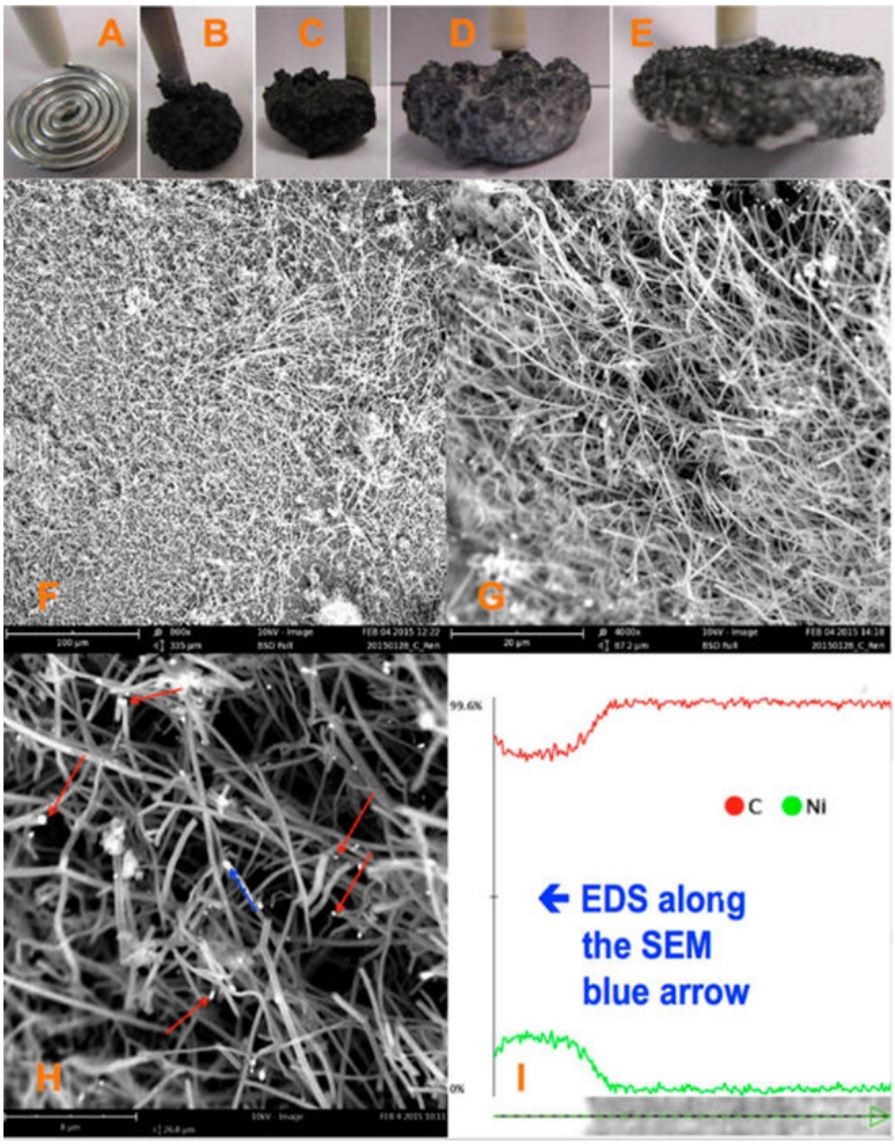

Fig. 5 (A) A 10 cm^2 coiled galvanized steel wire cathode before electrolysis; (B–E) Typical cathodes after electrolysis in molten carbonate. (F–H) Various magnifications SEM of the product. Red arrows in SEM "H" indicate Ni nucleation sites. The blue arrow indicates moving track of Ni site along the CNF; (I) EDS mapping of the 6 μm blue arrow path shown in SEM "H". Reprinted with permission from Ref. 34. Copyright 2015, American Chemical Society.

confirmed to be Ni by EDS measurement. The vast majority of the Ni nanoparticles in SEM are located at nanofiber tips, only a few seem to be aside from and not associated with CNF growth. The carbon fibers are homogeneous and have diameters of 200 to 300 nm, and length of 20 to 200 μm.

The linear EDS map in Fig. 5H shows Ni and C variation along the 6 μm path from pure Ni at the start of the fiber to pure carbon along the remainder of the fiber. The formation mechanism was proposed as: nickel (in this case originating from the Ni anode) first deposited on the cathode at initial low electrolysis currents (5 or 10 mA cm^{-2}) because of its low reduction potential and low solubility. This is evidenced by the observed low electrolysis voltage (<0.7 V). The formation of nickel metals appears to be crucial to induce CNF formation. In Li_2CO_3 melt, the electrolytic [CO_3^{2-}] has much higher concentration and faster mass diffusion than that of [Ni^{2+}], the carbonate reduction will be dominated at high currents electrolysis. The higher electrolysis voltage thermodynamically required to deposit carbon is observed at current of >20 mA cm^{-2}. Therefore, the initial low current nickel nucleation activation is necessary to form CNFs, instead, amorphous carbon will prefer to form. Interestingly, when Li_2O was added to the molten Li_2CO_3 electrolyte, tangled CNFs with a wide variety of diameters, instead of the straight/uniform diameter CNFs, were prepared as shown in Fig. 6. Consequently, the presence of high concentrations of oxide in Li_2CO_3 electrolyte leads to the formation of tangled CNFs.

In addition to Ni, further studies demonstrate that Cu, Co and Fe can also act as nucleation sites in the synthesis of cathodic product of CNFs during electrolysis in molten carbonates. The nucleation metals for CNFs growth were required to have a lower reduction potential at low current density than that required for carbon deposition. The metals of nickel, copper, iron, and cobalt enhancing the production of CNFs by

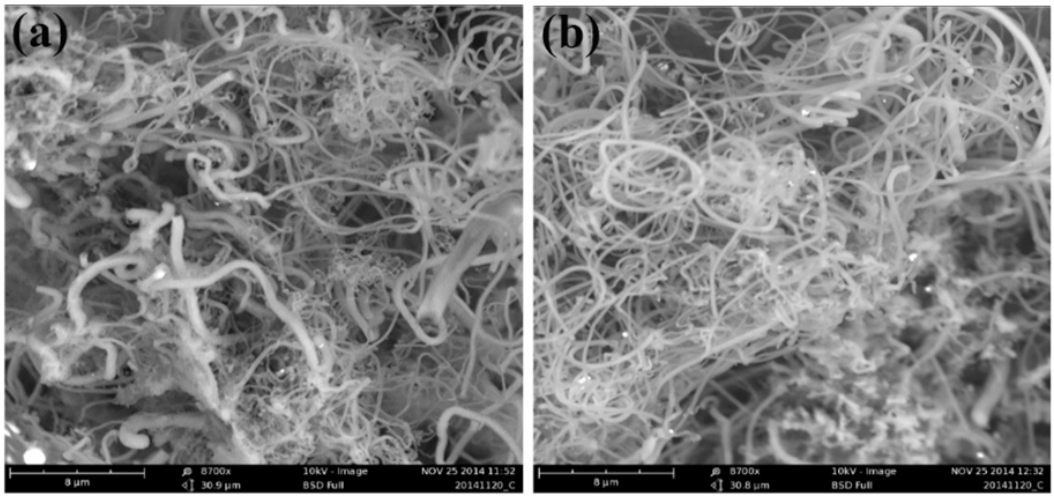

Fig. 6 SEM images of cathode product in 6M Li_2O/Li_2CO_3 electrolyte. Reprinted with permission from Ref. 34. Copyright 2015, American Chemical Society.

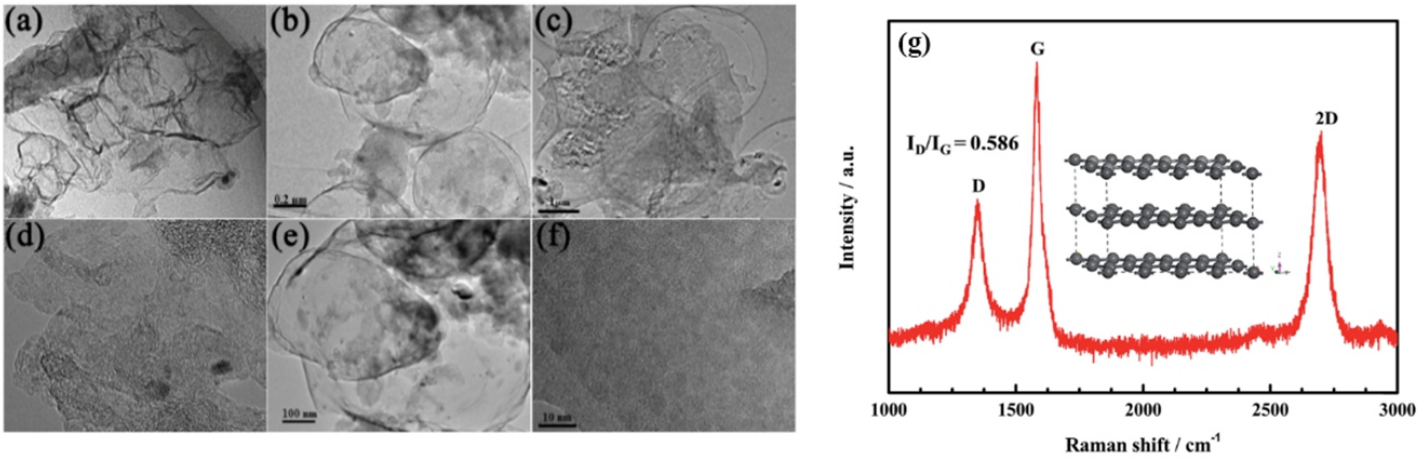

Fig. 7 TEM images of the products obtained on (a) stainless steel, (b) Cu, and (c) Ni electrode at 750 °C in $CaCl_2$–NaCl–CaO. HRTEM images of the product obtained on (d) stainless steel, (e) Cu, and (f) Ni electrode. Reprinted with permission from ref. 35. Copyright 2016, John Wiley & Sons, Inc. (g) Raman spectroscopy of obtained material. Reprinted with permission from Ref. 22. Copyright 2015, Royal Society of Chemistry.

molten electrolysis are also used as catalysts for CVD growth of CNFs.[69-71] Ni, Co, Cu or Fe was deposited at low current density from electrolytes which have a low concentration of the metal, and dissolved as oxide. The deposition of these nucleation sites on the cathode promote the CNFs formation and growth. In contrast, a solid metal cathode does not exhibit these characteristics and no homogeneous CNFs were formed. In the case of pure iron metal cathode, an overabundance of Fe results in uncontrolled carbon deposition and growth, which leads to the formation of randomly distributed (amorphous) carbon. Our group's results were further explored by other groups to control the diameter and length by means of tuning reaction time and catalyst particle size.[33,72-75]

Besides CNTs/CNFs, the efforts have also been made on the syntheses of graphene-like materials. Hu and co-workers systematically investigated the electrochemical reactions in a $CaCl_2$-CaO or $CaCl_2$-NaCl-CaO melt under CO_2 flow.[20,30,35] The anode is RuO_2·TiO_2 and various metals, including tungsten wire, Cu, stainless steel, Ni, were employed as the cathode. In both cases, a few layers of graphene could be produced as evidenced by TEM and Raman.[22,35]

The results showed that this process was temperature- and cathode-dependent. The carbon deposited at the stainless steel cathode at 750 °C (Fig. 7 a, d) has a "wrinkled sheet" structure that resembles graphene, while thick graphite flake and flat sheet with fewer layers were obtained at 650 °C and 850 °C, respectively. The product obtained on the Cu rod at 750 °C displays a special graphene ball structure with rolled edges (Fig. 7b, e). When Ni was used as a cathode, a flat-shaped graphene sheet with a few layers was observed (Fig. 7e, f). The results state clearly that the graphene structure is affected by the catalysis of metal atoms at the cathode. The mechanism was proposed to be metal-catalyzed deposition and micro-explosion of CO, as shown in Fig. 8. It should be noted if glassy carbon was employed as cathode, CNTs could be synthesized in $CaCl_2$-NaCl-CaO melt.[35]

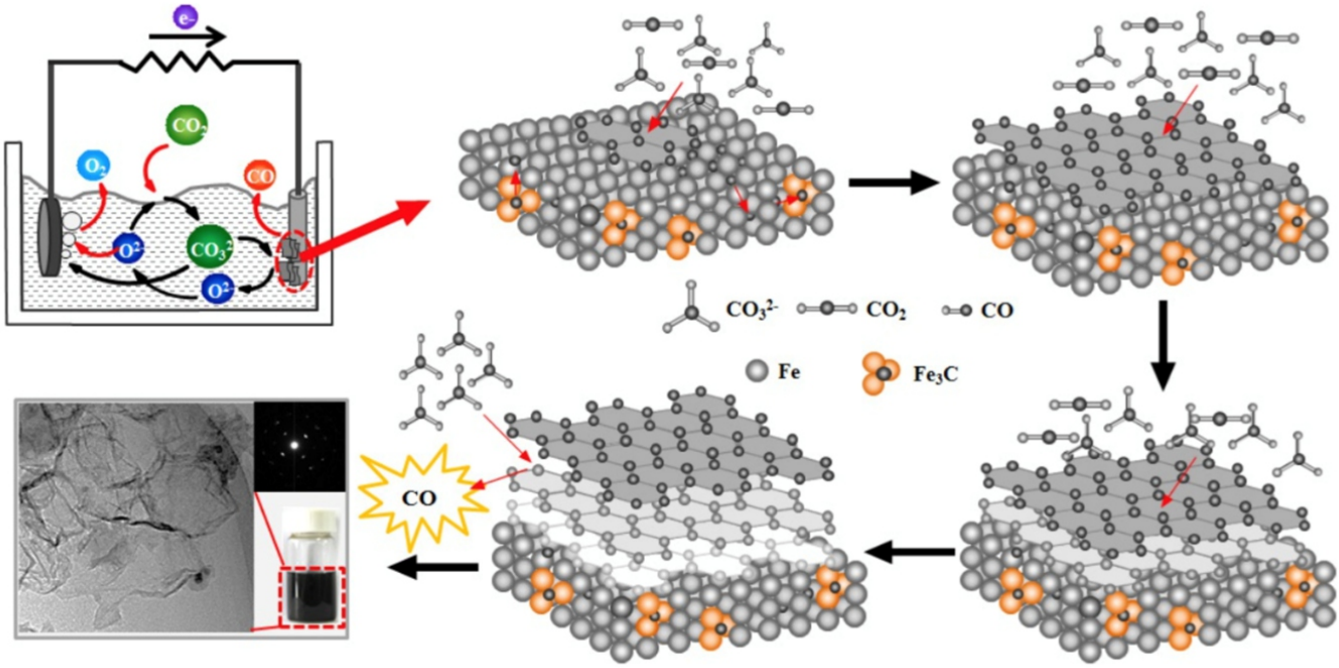

Fig. 8 The electrochemical synthesis of graphene on stainless steel cathode in molten $CaCl_2$–NaCl–CaO. Reprinted with permission from Ref. 35. Copyright 2016, John Wiley & Sons, Inc.

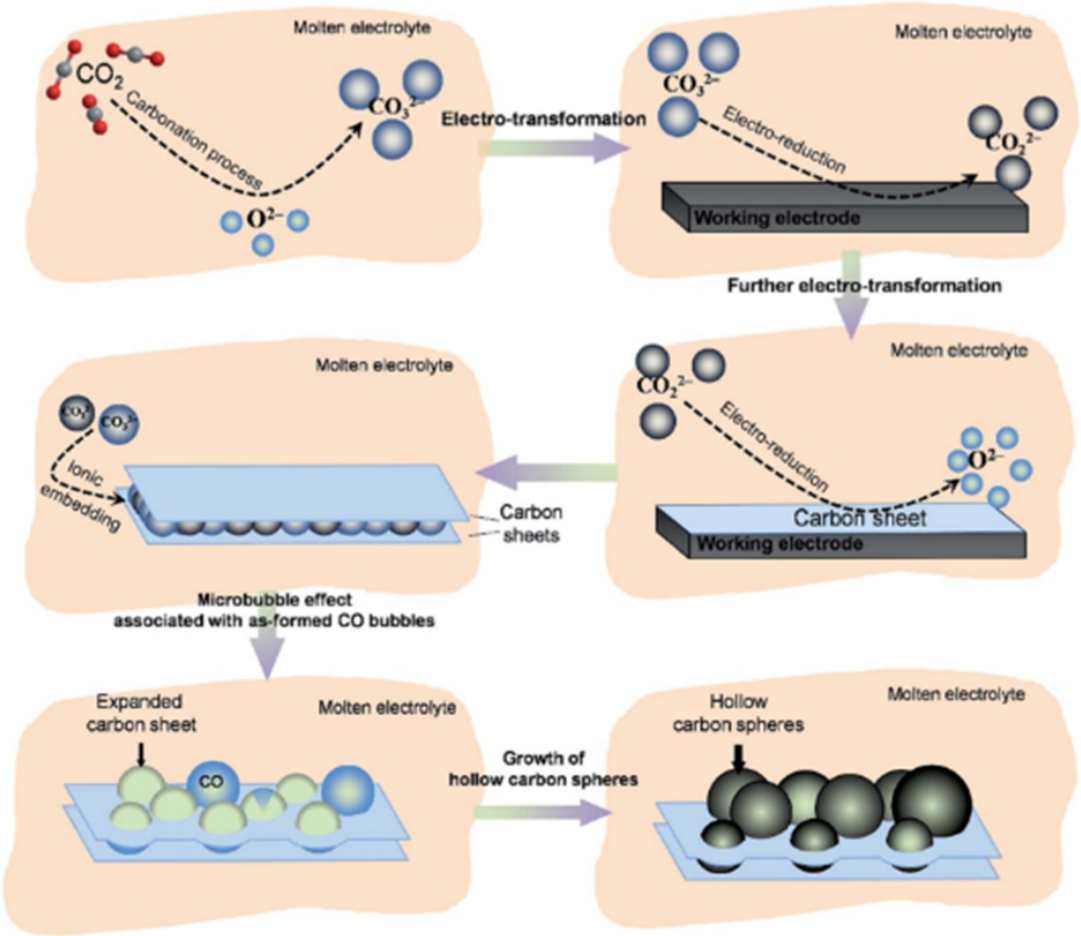

Fig. 9 Mechanism of the formation of hollow spheres. Reprinted with permission from Ref. 40. Copyright 2017, Royal Society of Chemistry.

In addition to CNTs and graphene, other types of carbon structures were also successfully produced via electro-reduction of CO_2. Typically, spherical, flake, random-shaped carbons were obtained. But some interesting materials were also obtained via this route. One-step high-yield synthesis of hollow carbon spheres by electrochemical reduction of CO_2 in a $CaCO_3$-LiCl–KCl melt at 450 °C was reported by Wang *et al*..[40] The formation mechanism was proposed as displayed in Fig. 9, by the following processes (1) formation of CO_3^{2-} via CO_2 absorption; (2) CO_3^{2-} was reduced to CO_2^{2-}; (3) CO_2^{2-} was further reduced to carbon and carbon sheets were deposited on the cathode during electrolysis; (4) remaining unreacted CO_2^{2-} or CO_3^{2-} was encapsulated into the carbon sheets and further reduced to CO; (5) the growing CO bubbles expand the carbon sheets to bubble-like structures; and (6) CO bubbles were further reduced to solid carbon and form hollow carbon sphere. It is worthwhile to note that growth of hollow carbon spheres deeply relies on the electrolyte composition and the precise control of electrode potential. The $CaCO_3$ in the melt (LiCl-KCl-$CaCO_3$) accounts for the release of CO and the resulting microbubble effect. If Li_2CO_3 was present instead of $CaCO_3$, CO was not found during electrolysis under temperature below 850 °C and the current of carbonate reduction in LiCl–KCl–$LiCO_3$ was much higher than that in LiCl–KCl–$CaCO_3$, which lead to the carbon products aggregating to form carbon nanoparticles instead of carbon hollow spheres. During the electrolysis in LiCl–KCl– Li_2CO_3, the fast conversion of CO_3^{2-} to C prevents the accumulation of unreacted CO_2^{2-}, thus, the reduction of CO_2^{2-} to carbon sheets and its subsequent microbubble effect would not occur.[40]

Nanostructured graphite was also prepared by the same group via the electrochemical reduction of molten Li_2CO_3–Na_2CO_3–K_2CO_3–Li_2SO_4 under synthetic flue gas flow (a mixture of CO_2 and SO_2) at a relatively low temperature of 775 °C[71]. The mechanism is relative complicated, but it is certain that this process is temperature dependent and without Li_2SO_4 in the liquid electrolyte and SO_2 in the gas, the graphitization could not happen. As proposed by the authors, the electro-reduction of sulfate ions to S^{2-} and S plays important role to de-oxygenate, and the in-situ SO_2 adsorption to form sulfate ions made this process to be a cycle. Sulfur can react with defective carbon in the matrix to form CS_2 resulting in the removal of imperfect carbons, and thus leads to a high degree of graphitization. Meanwhile, the S^{2-} ions facilitates the deoxygenation of graphite via reaction S + 2[O] → SO_2.[71] Therefore, sulfur assisted oxygen and defect carbon removal are favorable for the formation of high degree crystallize graphite on the cathode at a temperature of 775 °C.

Doped carbon materials exhibited enhanced properties, i.e. B-doped carbon for enhanced conductivity, N-doped carbon for high performance supercapacitor and excellent electro-catalytic activity, S-doped carbon for the heavy metal ion removal, etc.[31,76-78] The possibility of preparation of doped CNTs from CO_2 was explored by Ren *et al*. with the examples of B-, S-, and P-doped carbons by using Li_2CO_3 as

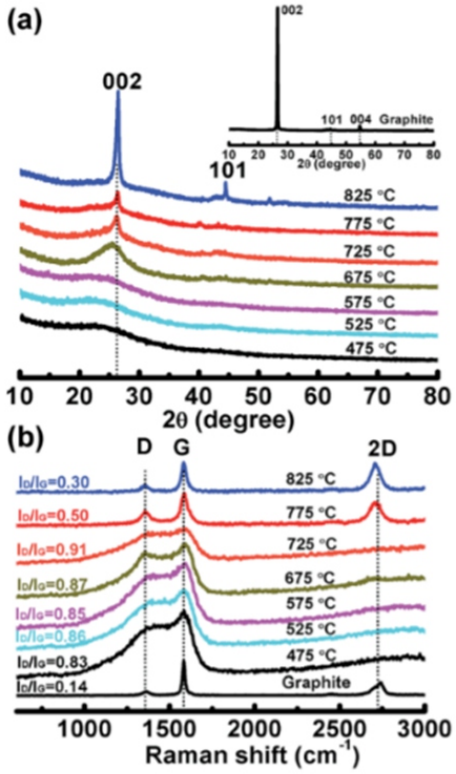

Fig. 10 (a) XRD and (b) Raman spectra of the commercial graphite and the electrolytic carbon materials obtained at different temperatures. Reprinted with permission from Ref. 71. Copyright 2017, Royal Society of Chemistry.

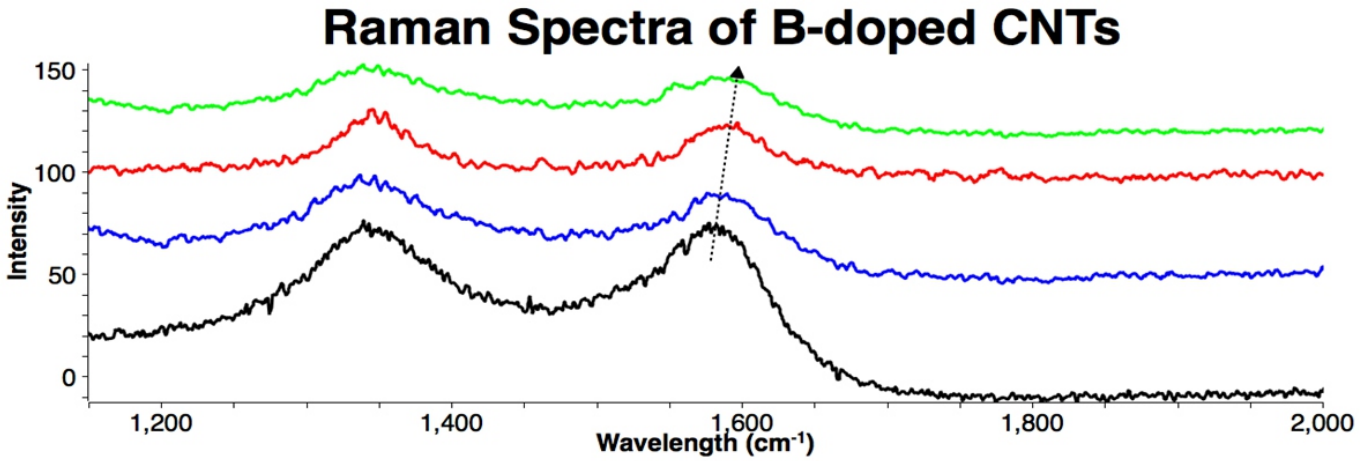

Fig. 11 Raman spectra of B-doped CNTs obtained from different $LiBO_2$ addition in 50g Li_2CO_3, from bottom to top the addition is 1.5g, 3g, 5g and 8g, respectively. Reprinted with permission from Ref. 31. Copyright 2017, Elsevier.

the electrolyte plus certain amount of $LiBO_2$ (Raman spectroscopy of B-doped CNTs in Fig. 11), Li_2SO_4 or $LiPO_3$.[31,79] The presence of B-, S-, and P-atom was confirmed by element analysis and Raman spectroscopy. However, their performances in adsorption, catalysis, etc., are still unknown.

5. Applications

Carbon materials are unique in energy storage because of their high surface area, excellent conductivity, strong resistance to acid/base/organic solvents, and tailorable crystal structures. The electrolytic carbons from CO_2 were tested in batteries and supercapacitors and displayed enhanced performances. The carbon materials prepared by electrochemical reduction of CO_2 in Li-Na-K carbonate melts were used as negative electrode materials for Li-ion batteries. A high reversible capacity of 798 mAh g^{-1} at 50 mA g^{-1}, which is more than two times higher than the theoretical capacity of graphite was achieved and it retains at 266 mAh g^{-1} over 500 cycles at a current density up to 500 mA g^{-1}.[80] Licht and co-workers also reported the results of electrolytic CNTs (straight and tangled) from CO_2 as the anode material in Lithium-ion and Sodium-ion batteries. Both straight (from pure Li_2CO_3 electrolyte) and tangled CNTs (from Li_2O/Li_2CO_3 electrolyte) displayed similar capacity of ~350 mAh g^{-1} in the initial 15 cycles in Li-ion battery test. After 200 cycles, the tangled CNT capacity increase to ~460 mAh g^{-1}, while the capacity of straight CNTs remains at ~360 mAh g^{-1}.[53] Such increased capacity during cycling has been reported in previous studies on carbon nanostructured electrodes, indicating the effect of the defect-induced modification to storage processes during cycling, particularly, with very high defect-containing carbons.[81] Based on the comparison of straight CNTs (I_D/I_G is 0.4 from Raman spectra) with tangled CNTs (I_D/I_G is 0.9 from Raman spectra), the high degree defects and bend in the tangled CNTs enable a transition from dilute staging of Li^+, which occurs during the formation of LiC_6, to a combination of this and the so called "intercalation and pore-filling" mechanism at defect sites.[81] The continuous activation of this storage mode enables a capacity superior to the maximum alloying capacity of Li in LiC_6.

However, in sodium-ion battery test, the charge-discharge behaviors are quite different between straight and tangled CNTs. The reversible capacity of the straight CNTs is only slightly higher than the maximum intercalation capacity of Na^+ in pure graphite. But the tangled CNTs show reversible capacities over 130 mAh g^{-1}, about two times higher than that of the straight CNTs. The results suggest that defects in CNTs (the tangled CNTs synthesized from the STEP process) are crucial to trigger the Na^+ storage. The in-situ adsorption and electrochemical reduction of CO_2 with STEP process provide a promising technology to develop high-performance carbon negative electrode materials for Li-ion batteries.[53]

When applying in supercapacitors, the capacitances of these electrolytic carbons in most reports are below 200 F/g. A very interesting report from Wang's group is sulfur-doped carbons prepared from the electrochemical reduction of molten Li_2CO_3–Na_2CO_3–K_2CO_3–Li_2SO_4 at 475 °C by using nickel and SnO_2 as the cathode and anode respectively[48]. The S-doped carbons exhibit high surface-area-normalized capacitance of 71.5 μF cm^{-2}, high gravimetric capacitance of 257.3 F g^{-1} and excellent cycling stability. This continuous-operation process is promising for massive preparation of advanced carbon materials for energy applications by the integration of carbon reduction and deep desulfurization from practical waste gas without purification. Additionally, carbons from CO_2 have been tested in other applications as well, such as the oxygen reduction and adsorption material for aqueous pollutants Cu(II) ion and methylene blue (MB).[82,83]

However, it is only in an early stage of the investigation of electrolytic carbons. Many possibilities may happen since this method can create carbons with controlled hetero-atom doping, controlled morphology, and high surface area.

6. Conclusion and future perspectives

As evidenced by latest studies, molten salts could be employed for better graphitization,[39] and create new materials by in-situ insertion of graphite. Electrochemical interaction between graphite and molten salts enables the preparation of carbon nanotubes, nanoparticles, graphene and nanodiamonds in molten salts. Electro-reduction of CO_2, either direct or indirect vs carbonate is versatile and powerful approach to create functional materials in a diversity of applications. More efforts should be made in (1) the defects control of electrolytic carbons, which is very important as electro-active materials, (2) detecting possibility of synthesis of SWCNTs or DWCNTs, fullerenes, Single layer or double layer graphene, etc., and (3) hetero-atom doped carbons.

Conflict of interest

There are no conflicts to declare.

Acknowledgements

We thank the financial supports from the National 1000 Young Talents Program of China and National Nature Science Foundation of China (Grant No. 21672076).

References

1. J. B. Smith, *Fisheries*, 1990, **15**, 2-6.
2. G. A. Meehl and W. M. Washington, *Nature*, 1996, **382**, 56-60.
3. H. Wu, D. Zou and K. Gao, *Sci. China Ser. C*, 2008, **51**, 1144-1150.
4. H. A. Hansen, J. B. Varley, A. A. Peterson and J. K. Nørskov, *J. Phys. Chem. Lett.*, 2013, **4**, 388-392.
5. D. Gau, R. Rodriguez, T. Kato, N. Saffon-Merceron, A. de Cózar, F. P. Cossío and A. Baceiredo, *Angew. Chem. Int. Ed.*, 2011, **50**, 1092-1096.
6. J. Bonin, M. Robert and M. Routier, *J. Am. Chem. Soc.*, 2014, **136**, 16768-16771.
7. P. G. Jessop, Y. Hsiao, T. Ikariya and R. Noyori, *J. Am. Chem. Soc.*, 1996, **118**, 344-355.
8. H. Li, P. H. Opgenorth, D. G. Wernick, S. Rogers, T. Y. Wu, W. Higashide, P. Malati, Y. X. Huo, K. M. Cho and J. C. Liao, *Science*, 2012, **335**, 1596-1596.
9. J. Albo, D. Vallejo, G. Beobide, O. Castillo, P. Castaño and A. Irabien, *Chem. Sus. Chem.*, 2017, **10**, 1100-1109.
10. C. S. Le Duff, M. J. Lawrence and P. Rodriguez, *Angew. Chem. Int. Ed.*, 2017, **129**, 13099-13104.
11. M. Gattrell, N. Gupta and A. Co, *J. Electroanal. Chem.*, 2006, **594**, 1-19.
12. Y. Koo, R. Malik, N. Alvarez, L. White, V. N. Shanov, M. Schulz, B. Collins, J. Sankar and Y. Yun, *RSC Adv.*, 2014, **4**, 16362-16367.
13. Y. Zhou, F. Che, M. Liu, C. Zou, Z. Liang, P. De Luna, H. Yuan, J. Li, Z. Wang, H. Xie, H. Li, P. Chen, E. Bladt, R. Quintero-Bermudez, T.-K. Sham, S. Bals, J. Hofkens, D. Sinton, G. Chen and E. H. Sargent, *Nat. Chem.*, 2018, **10**, 974-980.
14. H. Wu, D. Ji, L. Li, D. Yuan, Y. Zhu, B. Wang, Z. Zhang and S. Licht, *Adv. Energy Mater.*, 2016, **1**, 1600092.
15. H. R. M. Jhong, S. Ma and P. J. A. Kenis, *Curr. Opin. Chem. Eng.*, 2013, **2**, 191-199.
16. J. Qiao, Y. Liu, F. Hong and J. Zhang, *Chem. Soc. Rev.*, 2014, **43**, 631-675.
17. J. E. Bara, D. E. Camper, D. L. Gin and R. D. Noble, *Acc. Chem. Res.*, 2010, **43**, 152-159.
18. S. Licht, B. Wang, S. Ghosh, H. Ayub, D. Jiang and J. Ganley, *J. Phys. Chem. Lett.*, 2010, **1**, 2363-2368.
19. F. Haber and S. Tołłoczko, *Z Anogr. Allg. Chem.*, 1904, **41**, 407-441.
20. F. F. Li, S. Liu, B. Cui, J. Lau, J. Stuart, B. Wang and S. Licht, *Adv. Energy Mater.*, 2015, **5**, 1401791.
21. F. F. Li, J. Lau and S. Licht, *Adv. Sci.*, 2015, **2**, 1500260.

22. L. Hu, Y. Song, J. Ge, J. Zhu and S. Jiao, *J. Mater. Chem. A*, 2015, **3**, 21211-21218.
23. R. Ananthaiah, *Resonance*, 1997, **2**, 68-73.
24. R. J. Wilson, G. Meijer, D. S. Bethune, R. D. Johnson, D. D. Chambliss, M. S. de Vries, H. E. Hunziker and H. R. Wendt, *Nature*, 1990, **348**, 621-622.
25. S. Iijima, *Nature*, 1991, **354**, 56-58.
26. K. S. Novoselov, A. K. Geim, S. V. Morozov, D. Jiang, M. I. Katsnelson, I. V. Grigorieva, S. V. Dubonos and A. A. Firsov, *Nature*, 2005, **438**, 197-200.
27. Y. Zhang, Y. W. Tan, H. L. Stormer and P. Kim, *Nature*, 2005, **438**, 201-204.
28. P. Peng, F. F. Li, V. S. P. K. Neti, A. J. Metta-Magana and L. Echegoyen, *Angew. Chem. Int. Ed.*, 2014, **126**, 164-167.
29. P. Peng, D. Strohecker and Y. Liao, *Chem. Commun.*, 2011, **47**, 8575-8577.
30. L. Hu, Y. Song, J. Ge, J. Zhu, Z. Han and S. Jiao, *J. Mater. Chem. A*, 2017, **5**, 6219-6225.
31. J. Ren, M. Johnson, R. Singhal and S. Licht, *J. CO_2 Util.*, 2017, **18**, 335-344.
32. J. Ren and S. Licht, *Sci. Rep.*, 2016, **6**, 27760.
33. A. Douglas, N. Muralidharan, R. Carter and C. L. Pint, *ACS Sustain. Chem. Eng.*, 2017, **5**, 7104-7110.
34. J. Ren, F. F. Li, J. Lau, L. González-Urbina and S. Licht, *Nano Lett.*, 2015, **15**, 6142-6148.
35. L. Hu, Y. Song, S. Jiao, Y. Liu, J. Ge, H. Jiao, J. Zhu, J. Wang, H. Zhu and D. J. Fray, *Chem. Sus. Chem.*, 2016, **9**, 588-594.
36. A. R. Kamali, *Carbon*, 2017, **123**, 205-215.
37. A. R. Kamali and D. Fray, *J. Mater. Sci.*, 2016, **51**, 569-576.
38. A. R. Kamali and D. J. Fray, *Chem. Commun.*, 2015, **51**, 5594-5597.
39. X. Jin, R. He and S. Dai, *Chem. Eur. J.*, 2017, **23**, 11455-11459.
40. B. Deng, X. Mao, W. Xiao and D. Wang, *J. Mater. Chem. A*, 2017, **5**, 12822-12827.
41. B. Deng, Z. Chen, M. Gao, Y. Song, K. Zheng, J. Tang, W. Xiao, X. Mao and D. Wang, *Faraday Discuss.*, 2016, **190**, 241-258.
42. B. Deng, J. Tang, X. Mao, Y. Song, H. Zhu, W. Xiao and D. Wang, *Environ. Sci. Technol.*, 2016, **50**, 10588-10595.
43. Y. Yu, Z. Li, W. Zhang, W. Li, D. Ji, Y. Liu, Z. He and H. Wu, *New. J. Chem.*, 2018, **42**, 1208-1215.
44. H. V. Ijije, R. C. Lawrence and G. Z. Chen, *RSC Adv.*, 2014, **4**, 35808-35817.
45. D. Tang, H. Yin, X. Mao, W. Xiao and D. H. Wang, *Electrochim. Acta*, 2013, **114**, 567-573.
46. K. Du, K. Zheng, Z. Chen, H. Zhu, F. Gan and D. Wang, *Electrochim. Acta*, 2017, **245**, 410-416.
47. S. G. Kim, S. P. Yoon, J. Han, S. W. Nam, T. H. Lim, I.-H. Oh and S.-A. Hong, *Electrochim. Acta*, 2004, **49**, 3081-3089.
48. Z. Chen, B. Deng, K. Du, X. Mao, H. Zhu, W. Xiao and D. Wang, *Adv. Sustainable Syst.*, 2017, **1**, 1700047.
49. S. Licht, B. Wang and H. Wu, *J. Phys. Chem. C*, 2011, **115**, 11803-11821.
50. M. Johnson, J. Ren, M. Lefler, G. Licht, J. Vicini and S. Licht, *Data in Brief*, 2017, **14**, 592-606.
51. P. Bondavalli, C. Delfaure, P. Legagneux and D. Pribat, *J. Electrochem. Soc.*, 2013, **160**, A601-A606.
52. V. V. Srikanth, G. V. Ramana and P. S. Kumar, *J. Nanosci. Nanotechnol.*, 2016, **16**, 2418-2424.
53. S. Licht, A. Douglas, J. Ren, R. Carter, M. Lefler and C. L. Pint, *ACS Central Sci.*, 2016, **2**, 162-168.
54. H. Shi, Z. Fang, X. Zhang, F. Li, Y. Tang, Y. Zhou, P. Wu and G. Yu, *Nano Lett.* , 2018, **18**, 3193-3198.
55. R. Ma, L. Fan, S. Chen, Z. Wei, Y. Yang, H. Yang, Y. Qin and B. Lu, *ACS Appl. Mater. Inter.*, 2018, **10**, 15751-15759.
56. F. Xie, L. Zhang, C. Ye, M. Jaroniec and S. Z. Qiao, *Adv. Mater.*, 2018, 1800492.
57. S. Licht, M. Lefler, J. Ren and J. Vicini, *Mater. Sci.*, 2016, **1**, 55-63
58. C. Delacourt, P. L. Ridgway, J. B. Kerr and J. Newman, *J. Electrochem. Soc.*, 2008, **155**, B42-B49.
59. S. Zhang, P. Kang, S. Ubnoske, M. K. Brennaman, N. Song, R. L. House, J. T. Glass and T. J. Meyer, *J. Am. Chem. Soc.*, 2014, **136**, 7845-7848.
60. J. S. Yoo, R. Christensen, T. Vegge, J. K. Nørskov and F. Studt, *Chem. Sus. Chem.*, 2016, **9**, 358-363.
61. G. Ménard and D. W. Stephan, *J. Am. Chem. Soc.*, 2010, **132**, 1796-1797.
62. K. Le Van, H. Groult, F. Lantelme, M. Dubois, D. Avignant, A. Tressaud, S. Komaba, N. Kumagai and S. Sigrist, *Electrochim. Acta*, 2009, **54**, 4566-4573.
63. S. Licht, B. Cui and B. Wang, *J. CO_2 Util.*, 2013, **2**, 58-63.
64. J. Ren, J. Lau, M. Lefler and S. Licht, *J. Phys. Chem. C*, 2015, **119**, 23342-23349.
65. H. Z. Lu, X & Wang P., *TMS Annual Meeting*, 2009, 39-48.
66. A. Novoselova Inessa, F. Oliinyk Nikolai, B. Voronina Anastasiya and V. Volkov Sergei, *Z. Naturforsch A*, 2008, **63**, 467-474.
67. P. Queipo, A. G. Nasibulin, S. D. Shandakov, H. Jiang, D. Gonzalez and E. I. Kauppinen, *Curr. Appl. Phys.*, 2009, **9**, 301-305.
68. S. Boncel, S. W. Pattinson, V. Geiser, M. S. P. Shaffer and K. K. K. Koziol, *Beilstein J. Nanotech.*, 2014, **5**, 219-233.
69. T. W. Ebbesen, H. J. Lezec, H. Hiura, J. W. Bennett, H. F. Ghaemi and T. Thio, *Nature*, 1996, 382, 54-56.
70. Y. S. Song, J. R. Youn and T. G. Gutowski, *Compos. Part A-Appl. S*, 2009, **40**, 1257-1265.
71. Z. Chen, Y. Gu, L. Hu, W. Xiao, X. Mao, H. Zhu and D. Wang, *J. Mater. Chem. A*, 2017, **5**, 20603-20607.
72. A. Douglas and C. L. Pint, *ECS J. Solid State Sci. Technol.*, 2017, **6**, M3084-M3089.
73. A. Douglas, R. Carter, N. Muralidharan, L. Oakes and C. L. Pint, *Carbon*, 2017, **116**, 572-578.
74. A. Douglas, R. Carter, M. Li and C. L. Pint, *ACS Appl. Mater. Inter.*, 2018, **10**, 19010-19018.
75. S. Arcaro, F. A. Berutti, A. K. Alves and C. P. Bergmann, *Appl. Surf. Sci.*, 2019, **466**, 367-374.
76. H. Yu, L. Yang, D. Cheng and D. Cao, *Eng. Sci.*, 2018, **3**, 54-61.
77. L. Xiao, H. Xu, S. Zhou, T. Song, H. Wang, S. Li, W. Gan and Q. Yuan, *Electrochim. Acta*, 2014, 143, 143-151.
78. X. Wang, X. Zeng and D. Cao, *Eng. Sci.*, 2018, **1**, 55-63.
79. M. Johnson, J. Ren, M. Lefler, G. Licht, J. Vicini, X. Liu and S. Licht, *Mater. Today Energy*, 2017, **5**, 230-236.
80. J. Tang, B. Deng, F. Xu, W. Xiao and D. Wang, *J. Power Sources*, 2017, **341**, 419-426.
81. C. Bommier, T. W. Surta, M. Dolgos and X. Ji, *Nano Lett.*, 2015, **15**, 5888-5892.
82. Z. Chen, Y. Gu, K. Du, X. Wang, W. Xiao, X. Mao and D. Wang, *Electrochim. Acta*, 2017, **253**, 248-256.
83. X. Mao, Z. Yan, T. Sheng, M. Gao, H. Zhu, W. Xiao and D. Wang, *Carbon*, 2017, **111**, 162-172.